Macromolecules

pubs.acs.org/Macromolecules Article

Voltage-Triggered Structural Switching of Polyelectrolyte-Modified Nanochannels

Yamila A. Perez Sirkin, Igal Szleifer,* and Mario Tagliazucchi*

Cite This: Macromolecules 2020, 53, 2616−2626 Read Online

ABSTRACT: Synthetic solid-state nanochannels modified with polyelectrolyte brushes are an important class of stimuli-responsive nanofluidic devices. This work theoretically addresses the design of a voltage-triggered nanomechanical gate using the collapse transition of a hydrophobic polyelectrolyte brush within a long nanochannel. In poor solvent conditions, a polyelectrolyte brush grafted to the inner surface of a nanochannel can either collapse to its walls or stretch toward its axis in order to form a central dense plug. An applied transmembrane potential favors polyelectrolyte chain conformations that are tilted in the direction of the electric field, and therefore, the transmembrane potential can trigger a transition from the collapsed-to-the-center state to the collapsed-to-the-wall state. This work studied this transition as a function of the length of the polyelectrolyte chains, the hydrophobicity of the polymer backbone, and the pH and ionic strength of the solution. The optimal conditions to achieve a sharp voltage-triggered transition between the collapsed-to-the-wall and the collapsed-to-the-center structures were identified. This work also explored the effect of the voltage-triggered collapse transition on the transport of probe particles of different sizes. It is shown that there is a balance between the permeability of the channel and the selectivity of the two different collapse states for the particular system explored in this work. This balance makes the structural transition mostly effective to gate the transport of species within the ~1 nm range.

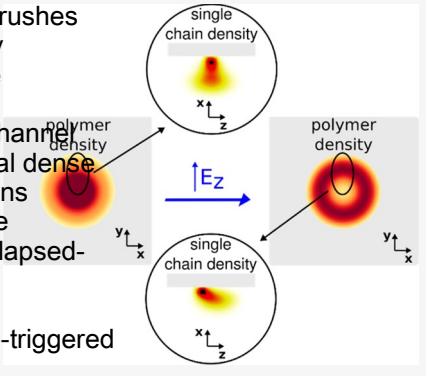

INTRODUCTION

The transport of ions through biological nanopores and nanochannels is a complex phenomenon whose selectivity is granted by the interactions between the ion and the amino acids lining the internal surface of the channel.[1,2] Biological channels have the ability to allow or block the translocation of ions by switching between open and closed states in response to chemical stimuli or changes in the membrane potential.[2−7] These channels have inspired synthetic nanopores and nanochannels that aim to reproduce the transport selectivity[1,2,8] and gating behaviors[9,10] found in nature. In particular, the types of stimuli that can gate transport in synthetic nanochannels have impressively grown over the last years.[11−15]

The transmembrane potential is an atypical stimulus because it can modulate the conductivity of current-rectifying nanochannels, and it is, at the same time, the driving force for ion transport. Current-rectifying nanofluidic elements exhibit large currents in their open state and, upon reversing the polarity of the applied electric potential, low currents in the closed state.[16,17] Current rectification requires an asymmetric charge distribution with respect to the plane of the membrane, which can be achieved either by introducing an asymmetric surface charge in a shape-symmetric nanochannel (i.e., a cylindrical channel),[18,19] by having a shape-asymmetric channel (i.e., conical or bullet-shaped channels) with a homogeneous surface charge,[20−24] or by using solutions of different compositions in the reservoirs.[20,25] In all these cases, current rectification results from the redistribution of the ion concentrations within the system as a function of the applied potential.[15,17,26] In other words, the concentrations of the ions in each position within the system are different in the open and closed states. These differences in the concentration profiles are responsible for the different conductances of these two states.

Grafting polyelectrolyte chains to the inner walls of synthetic nanochannels is a common strategy to tune their transport properties.[14,21,27−30] Previous work of our group has shown that the structure of short nanopores modified by polyelectrolyte brushes gradually deforms as the applied potential is increased.[31] In the presence of an applied potential, polyelectrolyte chains tend to stretch in the direction of the reservoir that has an opposite electric charge to that of the polyelectrolyte. Voltage-driven deformation of grafted polyelectrolyte chains has also been proposed by Siwy and co-workers to explain their experimental current−potential curves in DNA-modified nanopores.[32−34] The deformation of the polyelectrolyte brush in response to the applied trans-

Received: January 12, 2020
Revised: March 4, 2020
Published: March 24, 2020

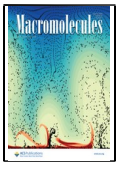

https://dx.doi.org/10.1021/acs.macromol.0c00082
Macromolecules 2020, 53, 2616−2626

membrane potential affects the ionic currents within the channel,[31,32,34] both due to electrostatic and steric interactions. In the case where the steric interactions dominate, the system is a voltage-triggered nanomechanical gate, whose conduct can be opened or blocked in response to changes in the applied transmembrane potential.[34]

The biological counterparts of the artificial voltage-gated nanochannels discussed above are the voltage-gated ion channels. This important class of transmembrane proteins can open/close as a response of the transmembrane potential. The combination of exquisite ion-transport selectivity (i.e., Na^+ vs K^+)[2] and gating by voltage enables very selective voltage-activated ion fluxes, which change the state of polarization of the membrane and, ultimately, trigger action potentials and nerve impulses. The gating mechanism in biological channels involves a conformational change in the channel induced by the electric field across the membrane.[35] For example, in K^+ voltage-gated ion channels, the electric field across the membrane interacts with an α-helix rich in positively charged amino acids (S4 helix).[7,35] The interaction of the electric field with this voltage-sensing residue triggers a conformational change that modifies the conductivity state of the channel. Note that while in synthetic current-rectifying channels the voltage-dependent conductance results from the reorganization of the ion concentrations within the system (i.e., a reorganization of the local concentrations of the species being transported), in biological ion channels, the voltage-gated conductance is a result of structural changes in the channel itself (i.e., a reorganization of the environment responsible for transport). Because of these fundamental differences, single voltage-gated biological channels exhibit sharp on−off transitions,[7] whose probability depend on the transmembrane potential. On the other hand, man-made ion-rectifying nanochannels show gradual conductance changes with the transmembrane potential. A key question is how sharp voltage-triggered structural changes can be produced in an artificial nanochannel with a diameter much larger than the size of a single ion. In this work, we propose to use the hydrophobic collapse of a polyelectrolyte brush in poor solvent conditions (i.e., its microphase separation)[36] for this end.

End-grafted layers of polymers or polyelectrolytes with hydrophobic backbones can aggregate in micro-/nanostructures of different morphologies in order to avoid contact with the solvent.[36,37] Changes in the effective segment−segment attractive strength, by changing either the quality of the solvent or the average charge per monomer, result in steep transitions between self-assembled nanostructures with different morphologies. When the polymer layer is confined within a nanochannel, there is a particularly interesting morphological transition between structures that are collapsed on the channel's inner walls (collapsed-to-the-wall states) and structures in which the polymer chains collapse to the axis of the channel, forming a central plug (collapsed-to-the-center state).[37−39] The conductance behavior of channels modified by pNIPAM brushes has been associated with the existence of these two collapse configurations.[28,40] In another example, Speyer and Pastorino studied the transition between the two collapse states induced by an applied pressure using molecular dynamics simulations.[39] Based on these previous works, the transition between the collapsed-to-the-center and collapsed-to-the-wall states emerges as an interesting strategy to create nanochannels with sharp stimuli-induced structural transitions.

In this work, we theoretically design a nanochannel bearing positively charged polyelectrolyte chains that shows a sharp structural transition with the applied transmembrane potential. Figure 1 shows a scheme of the proposed design. We consider

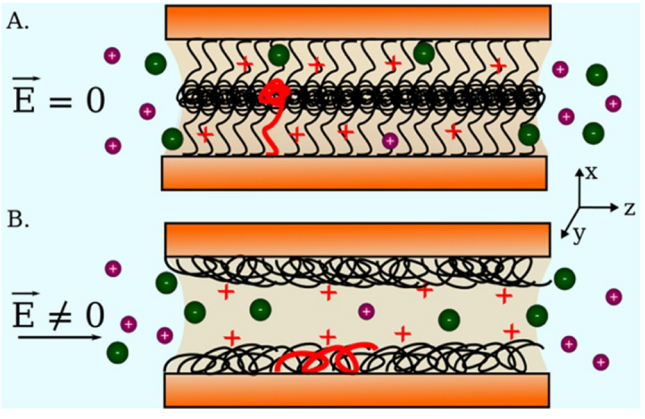

Figure 1. Scheme of proposed design of a voltage-triggered nanomechanical gate. A cylindrical nanochannel of radius R and length L (R ≪ L) is modified with a brush of a weak polybase with a hydrophobic backbone (i.e., the backbone is in poor solvent conditions). The nanochannel connects two identical reservoirs of an aqueous solution containing salt anions and cations, and H^+ ions. In the proposed design, the polyelectrolyte is collapsed to the axis of the channel (collapsed-to-the-center state) in the absence of an applied potential (panel A). After applying a large enough potential between electrodes in the reservoirs, the force exerted by the electric field on the polybase chains is expected to trigger a conformational transition to the collapsed-to-the-wall state (panel B). In each panel, one polymer chain is shown in red to empathize the conformational change.

a single cylindrical nanochannel (radius ≪ length) in a membrane separating two identical reservoirs. A potential ΔV is applied between electrodes in each of the reservoirs. We refer to this potential as the transmembrane potential because the access resistance is much smaller than the channel resistance for this system,[31] and therefore, there is no Ohmic drop in the reservoirs and the potential difference across the membrane is ΔV. The inner surface of the nanochannel is coated by a brush of a pH-responsive positively charged polyelectrolyte, whose backbone is in poor solvent conditions, and therefore, the uncharged state of the polyelectrolyte is poorly soluble in water. One example of a polyelectrolyte with these properties is 4-poly(vinylpyridine).[37] The pH of the system is tuned to allow hydrophobic interactions to dominate over electrostatic repulsions and, therefore, collapse the polyelectrolyte brush.[36] Moreover, by proper choice of the polyelectrolyte chain length, the collapse occurs in the center of the channel in equilibrium conditions (collapsed-to-the-center state at zero applied potential, see Figure 1A). Upon increasing the transmembrane potential, the electric field within the channel (sustained by an ionic current) stretches the polyelectrolyte chains and tilts them in the axial direction. At a given threshold potential, the electrophoretic force exerted by the electric field on the polyelectrolyte chains is expected to trigger a transition from the collapsed-to-the-center state to the collapsed-to-the-wall state (see Figure 1B). We theoretically studied this system with a molecular theory,[31,41,42] which explicitly considers the molecular details of all chemical species in the system, their intra- and intermolecular interactions, and

https://dx.doi.org/10.1021/acs.macromol.0c00082
Macromolecules 2020, 53, 2616−2626

the presence of the coupled acid−base equilibrium (see the Theoretical Methods section and Supporting Information). The theory used in this work is a nonequilibrium molecular theory[31,42] because it models the system in the presence of steady-state ionic current. We used the theory to find the optimal conditions for the voltage-gated transition from the collapsed-to-the-center to the collapsed-to-the-wall state and to evaluate if this transition can be used to control the translocation of probe particles of different sizes.

THEORETICAL METHODS

The theoretical tool used in this work is a molecular theory that explicitly incorporates molecular details of the system such as the size, shape, charge, charge distribution, and conformations of all molecular species in the system. It also considers the intra- and intermolecular interactions among these species and the presence of coupled chemical equilibria. In previous works, the predictions of the molecular theory were found to be in excellent agreement with experiments.[41,43,44] We will provide in this section an outline of the theoretical framework used in this work, but we refer the reader to the Supporting Information for a detailed description of the theory, the molecular model, and the methodology used for obtaining the numerical solutions.

The formulation of the theory is based on a previously developed nonequilibrium molecular theory,[31,42] which follows the ideas of local equilibrium approximation.[45,46] This approximation states that the equilibrium relationships between thermodynamic variables in a nonequilibrium system hold approximately at a local length scale. Assuming steady-state conditions (the properties of the system do not depend on time), the starting point of the nonequilibrium molecular theory is a generalized form of Fick's second law of diffusion, which relates the mass fluxes in the system with gradients of the chemical potentials of the corresponding species.

$$\frac{\partial \rho_i(\mathbf{r})}{\partial t} = -\nabla \cdot J_i(\mathbf{r}) = \nabla[D_i \rho_i(\mathbf{r}) \nabla \beta\mu_i(\mathbf{r})] = 0 \quad (1)$$

where i = A, C, H^+, or OH^- for the anions, cations, protons, and hydroxyl ions, respectively, r is the position vector, that is, r = (x, y, z), D_i is the diffusion coefficient for the different species, $\rho_i(r)$, and $\mu_i(r)$ are the density and chemical potential of the species i at position r, respectively, and $\beta = 1/k_BT$, where k_B is Boltzmann's constant and T is the temperature.

Our approach to obtain an expression for $\rho_i(r)$ and solve the molecular organization of the system is to write down an expression for the semi-grand canonical free-energy potential of the system, which describes a system with fixed chemical potential for the ions and fixed number of polymer chains. In the present case, the semi-grand canonical functional is

$$\begin{aligned}\beta\Omega = & \int \rho_s(\mathbf{r})[\ln(\rho_s(\mathbf{r})\upsilon_s) - 1]\,d\mathbf{r} \\ & + \sum_{i=A,C,H^+,OH^-} \int \rho_i(\mathbf{r})[\ln(\rho_i(\mathbf{r})\upsilon_s) - 1 + \mu_i^0]\,d\mathbf{r} \\ & + \rho_G \int \sum_{\alpha} P_P(\mathbf{r};\alpha)\ln(P_P(\mathbf{r};\alpha))\,d\mathbf{s} \\ & + \int\int \frac{\beta\chi g(|\mathbf{r}-\mathbf{r}'|)}{2} \langle n_P(\mathbf{r})\rangle\langle n_P(\mathbf{r}')\rangle\,d\mathbf{r}\,d\mathbf{r}' \\ & + \int (\langle\rho_Q(\mathbf{r})\rangle\beta\psi(\mathbf{r}) - \frac{1}{2}\varepsilon\beta(\nabla\psi(\mathbf{r}))^2)\,d\mathbf{r} \\ & + \int \langle n_P(\mathbf{r})\rangle[f(\mathbf{r})\ln(f(\mathbf{r})) + (1-f(\mathbf{r}))\ln(1-f(\mathbf{r}))]\,d\mathbf{r} \\ & + \int \langle n_P(\mathbf{r})\rangle[f(\mathbf{r})\beta\mu_{BH^+}^0 + (1-f(\mathbf{r}))\beta\mu_B^0]\,d\mathbf{r} \\ & - \sum_{i=A,C,H^+,OH^-} \int \rho_i(\mathbf{r})\beta\mu_i(\mathbf{r})\,d\mathbf{r} \\ & - \int (1-f(\mathbf{r}))\langle n_P(\mathbf{r})\rangle\beta\mu_{OH^-}(\mathbf{r})\,d\mathbf{r}\end{aligned} \quad (2)$$

The first two terms in the right hand of eq 2 represent the translational or mixing entropy of the solvent and ions, respectively. The third term is the conformational entropy of the polyelectrolyte chains, and the fourth term is the effective attractive energy between polymer beads that represents the hydrophobicity of the backbone. The fifth term is the electrostatic energy of the system. The sixth and seventh contributions to Ω are the chemical free energy of the acid−base reactions. The last two terms result from the fact that Ω is a grand canonical potential with respect to the mobile ions (our semi-grand canonical potential does not include intermolecular steric repulsions which are accounted for through a packing constraint.

The semi-grand potential Ω depends on functions that define the structure of the system and are a priori unknown, such as the number density of solvent and ions at each position, $\rho_i(r)$, with i = solvent, C, A, H^+, OH^-; the position-dependent electrostatic potential, ψ(r); the fraction of protonated polymer segments at r, f(r); and the probability distribution function of the polymer chain conformations, $P_P(s,\alpha)$. Note that in eq 2, the chemical potentials of the ions, $\mu_i(r)$, depend on the position within the system because the system is in a nonequilibrium steady state rather than in equilibrium (where it should be constant). The functional extrema of eq 2 with respect to the unknown functions mentioned above provides analytical expressions for them. The resulting set of equations, including the equations that describe the fluxes in the system (eq 1), is solved using numerical methods in order to obtain the nonequilibrium steady-state structure of the system and the fluxes of ions.

A main characteristic of the molecular theory is that all interaction fields and the distribution and chemical states of all species are highly coupled, thus the equations of the theory are solved self-consistently. In the case of the nonequilibrium molecular theory, structure and ion transport in the system are also coupled, and therefore, they should be solved self-consistently (see ref 31). However, in the particular case of a very long nanochannel discussed in the present work, it is possible to decouple these two aspects of the problem, which greatly simplifies its computational treatment (see Long-Nanochannel Approximation in the Supporting Information). Decoupling of structure and transport requires to neglect concentration changes and Ohmic drops at the reservoirs, which is a very good approximation for very long channels.[31] Under this approximation, the densities of ions, solvent, and polymer within the very long nanochannel are homogeneous in the z (axial) direction and inhomogeneities in the y,x plane. The long-nanochannel approximation allows us to map the (computationally demanding) problem of calculating the steady-state properties of the three-dimensional system into an equilibrium calculation on the cross-sectional area of the channel. The latter calculation differs from

https://dx.doi.org/10.1021/acs.macromol.0c00082
Macromolecules 2020, 53, 2616−2626

a standard equilibrium calculation[47] in an additional term included in the calculation of the probability of each chain conformation that accounts for the force exerted by the electric field on the charges of the polyelectrolyte. It should be stressed that the long-channel approximation used in this work is invalid for short channels, for which structure and transport are irremediably coupled (see ref 31).

The molecular theory has some limitations and approximations, which are important to discuss. First, there are approximations inherent to the theory, such as treating intermolecular interactions in a mean-field approximation and using a coarse-grained model for the polymer. The validity of these approximations is empirically supported by the good agreement between theory and experiment for several soft-matter systems,[41,44,48,49] including polymer-modified nanochannels.[41,49] A specific approximation involved in the present formulation of the theory is that of homogeneity in the axial direction. This approximation is reasonable for the very long nanochannels studied here, although it has the disadvantage of precluding microphase separation (aggregate formation) in the axial direction. In a previous paper,[37] we showed that the translational symmetry of the system can be broken by polymer collapse, which creates inhomogeneities along the axial coordinate (z). In the present case, such symmetry breaking is forbidden by the assumption of homogeneity in the axial direction. However, in ref 37, we also showed that the aggregates formed by brushes microphase-separ in the axial direction have collapsed-to-the-center and collapsed-to the-wall states. Therefore, the main conclusions of the present paper will be valid even for a channel where aggregate formation also oc in the axial direction. The current formulation of the molecular theo also neglects electroosmotic flows. The importance of electroosmotic flows decreases for increasing channel length,[50] and hydrodynamic friction with the polymer brush will also reduce solvent flows; thus, believe that neglecting electroosmotic flow is not a critical for the very long polymer-modified channels considered here. Finally, we neglected heat production inside the nanochannel because of the Joule effect. This effect can be relevant in microchannels,[61] which can sustain large currents (i > 1 mA); however, it is negligible in nanochannels, where currents are of the order of the nanoamperes.

RESULTS AND DISCUSSION

Structure of the Nanochannel in Equilibrium (Zero Transmembrane Potential). The organization of a polyelectrolyte brush within a nanochannel is a complex function of its radius, the length of the polymeric chains, the quality of the solvent, and the pH and salt concentration of the solution.[31,37−39,41,42,52] In order to find the optimal conditions for the nanomechanical gate proposed in Figure 1, we will first explore the effects of channel radius and chain length in the absence of an applied potential (equilibrium state). This analysis will provide the conditions to form the collapsed-to-the-center state. In a second step, we will scan the pH and salt concentration to find the threshold conditions under which the system transitions to the collapsed-to-the-wall state. The rationale behind this approach is that the voltage-gated transition from the collapsed-to-the-center to the collapsed-to-the-wall structure will be optimal when the system is in its most sensitive state, that is, when the polyelectrolyte is collapsed to the center but a small change in variables such as pH or ionic strength will trigger a transition to the collapsed-to-the-wall state.

We consider here a very long channel (L ≫ R) and use the approximation that all structural properties of the system are homogeneous in the axial direction (all properties are invariant with translations along the z-axis). Note that this approximation does not preclude the polyelectrolyte chains to stretch in the axial direction in the presence of the electric field because, even though we assume homogeneity in the axial direction, we still keep track of the fully three-dimensional coordinates of all segments of each polyelectrolyte conformation. Therefore, an electric field in the axial direction increases the probability of those conformations that are tilted in the direction of the field. As we explain in the Theoretical Methods section and the Supporting Information, the long-channel approximation allows us to decouple the problems of ion transport and polyelectrolyte organization, which makes the present system computationally tractable.

The collapse behavior of neutral polymer brushes in channels with rotational (axisymmetric)[37] and axial (translational)[38] symmetries in equilibrium has been already discussed in detail in the literature, so we will limit the discussion to a few cases of interest for the design of the voltage-triggered nanogate. In Figure 2, we present the equilibrium (zero applied electric field) structure of the polyelectrolyte as a color map of the polymer volume fraction (fraction of the volume occupied by polymer segments) in the plane normal to the axis for different nanochannel radii and chain lengths in good solvent conditions (Figure 2A), we observe a transition from a partially occluded channel for short chains (N = 20 for R = 5 nm and N = 40 for R = 8 nm) to a homogeneously occluded channel for long chains (N = 40 for R = 5 nm and N = 70 for R = 8 nm). The maximum volume fraction inside the channel in the latter case is rather low (ϕ_P ≈ 0.1. This result is consistent with a brush that is fully extended in order to minimize electrostatic repulsions.

On the other hand, in poor solvent conditions (Figure 2B), the structure of the polyelectrolyte brush collapses to increase the number of segment−segment contacts. For short polymers,

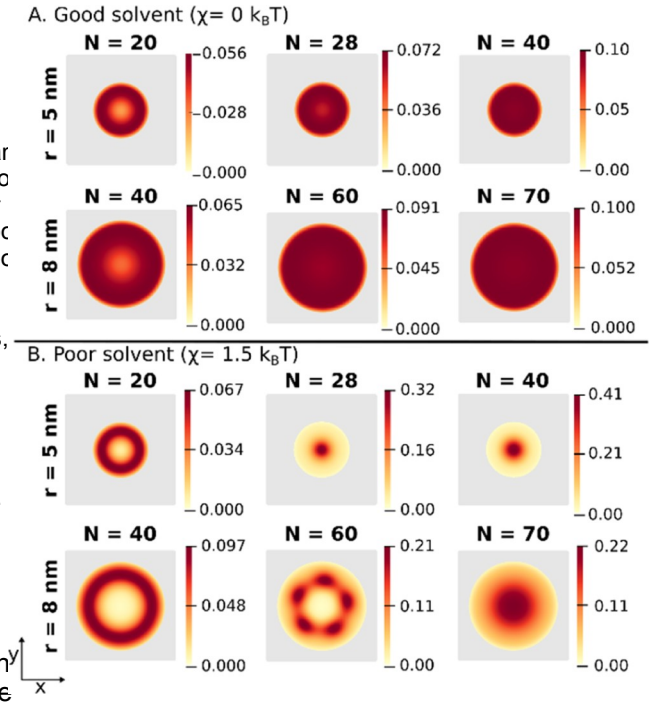

Figure 2. Color maps of the polyelectrolyte volume fraction on a plane normal to the channel axis. The figure shows the effect of the radius of the nanochannel and chain length on the morphology of the polymer brush. System conditions: pH = 8.5, pK_a = 8, surface coverage = 0.05 chains/nm^2, and salt concentration = 0.1 M. (a,b) Cases of hydrophilic (χ = 0) and hydrophobic (χ = k_BT) polymer backbones, respectively (good and poor solvent conditions).

https://dx.doi.org/10.1021/acs.macromol.0c00082
Macromolecules 2020, 53, 2616−2626

the preferred aggregation mechanism collapses to the nanochannel walls, while increasing the polymer chain length favors collapsing to the channel axis. This result is in good agreement with the experimental observations of Zhang et al.,[53] who proposed the existence of the two different collapse states to explain the different gating behaviors observed for nanochannels grafted with pNIPAM brushes of different chain lengths. Interestingly, in some conditions, we observe that polymer collapse breaks the rotational symmetry of the system (see Figure 2B for R = 8 nm and N = 60). This result is in agreement with previous theoretical predictions.[38] Increasing the radius of the channel favors symmetry breaking in the angular coordinate (such as that observed in Figure 2B) because the increase in the circumference provides additional room for the formation of individual polyelectrolyte aggregates.

Based on the results of Figure 2, we decided to explore the effect of the applied potential for R = 5 nm (to avoid the additional complexity of structures with broken angular symmetry) and an intermediate chain length, N = 28, to be near to the transition from the collapsed-to-the-center to the collapsed-to-the-wall state. Using these parameters, we studied the balance between electrostatic interactions (controlled by the solution pH, lower pHs correspond to stronger electrostatic repulsions) and hydrophobic interactions (controlled by the segment−segment attraction strength χ, higher χ indicates stronger hydrophobic attractions). Figure 3 shows the effect of pH and χ on the structure of the polymer layer. Three well-defined regimes are apparent. In the first regime, the solvent is good for the polymer backbone (χ = 0), and, as shown above, the polyelectrolyte chains stretch in order to reduce electrostatic repulsions. For strong segment−segment attractions (large χ) and/or low charge density (high pH), the system adopts the most compact conformation, which corresponds to the collapsed-to-the-center state. Between these two limiting scenarios, we observe the collapsed-to-the-wall structure. Note that the collapsed-to-the-center state exhibits a larger maximum volume fraction (i.e., it is more compact) than the collapsed-to-the-wall state.

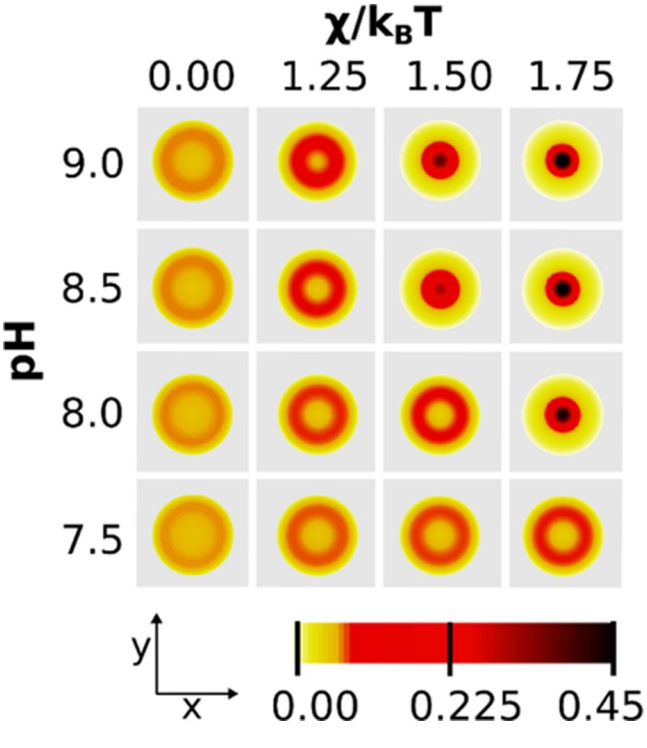

Figure 3. Color maps of the polyelectrolyte volume fraction on a plane normal to the channel axis as a function of the solution pH and the hydrophobicity of the polyelectrolyte backbone, χ (larger values of χ indicate stronger segment−segment hydrophobic attractions). Conditions: R = 5 nm, N = 28, pH = 8.5, pK_a = 8, surface coverage = 0.05 chains/nm^2, and salt concentration = 0.1 M.

Using the results of Figure 3, we aimed to choose the conditions that minimize the applied potential required to trigger the transition between the two collapsed states. These conditions will correspond to a system that is in the collapsed-to-the-center state but near the threshold to the transition to the collapsed-to-the-wall morphology. In an experimental realization, the interaction strength χ will be fixed by the chemistry of the polymer, but the solution pH can be easily controlled. Assuming a value of χ = 1.5 k_BT, we choose the minimum pH required to obtain the collapsed-to-the-center structure in Figure 3, pH = 8.5. These values of χ and pH were used to analyze the effect of an external applied bias on polymer conformation in the next section. The final combination of χ, pH, chain length, and channel radius that will be used in the next section is, of course, not unique: the voltage-triggered transition can be found for other combinations as well; however, we believe that our strategy to find the best conditions for the voltage-triggered structural transitions is general and potentially useful in both experimental and theoretical approaches. The charge of the polyelectrolyte is an important additional design parameter that controls the sharpness of the structural transition because a certain number of charges are required to couple with the external electrical field, but too many charges will increase electrostatic repulsions between chains and prevent the collapse of the brush. Thus, for highly charged polyelectrolytes, we do not observe a sharp conformational transition but rather a smooth reorganization of the layer with the applied potential, similar to that already reported in ref 31.

Structure of the Nanochannel in the Presence of an Applied Transmembrane Potential. We will now consider the effect of an electric field in the axial direction (which results from applying a potential bias between the reservoirs) on the structure of the polyelectrolyte layer. Note that this electric field creates ionic currents in the system; therefore, the system is in a steady state rather than in equilibrium.[31] The starting conformation corresponds to the case pH = 8.5 and χ = 1.5 k_BT in Figure 3, which is a collapsed-to-the-center structure. Figure 4A shows that for a salt concentration of 0.1 M (same salt concentration as in Figure 3), there is a sudden transition from the collapsed-to-the-center state to the collapsed-to-the-wall state upon increasing the strength of the applied electric field. The transition occurs between E = 1.03 and 1.29 V/μm. Detailed calculations show that the exact threshold for this transition is E = 1.09 V/μm. For a typical nanochannel membrane of L = 10 μm prepared by etching of an ion track,[15] the transition will require an applied potential between the electrodes in the reservoirs of ΔV = 10.9 V, which is in the upper limit of those typically used to probe these systems.[54] This argument assumes that all the Ohmic drop occurs within the channel, neglecting the access resistances, which is an excellent approximation for long channels.[31,50] The transmembrane potential required for the transition, ΔV = E.L, can be decreased by using channels shorter than 10 μm; however, for very short pores, the Ohmic drop in the reservoirs

https://dx.doi.org/10.1021/acs.macromol.0c00082
Macromolecules 2020, 53, 2616−2626

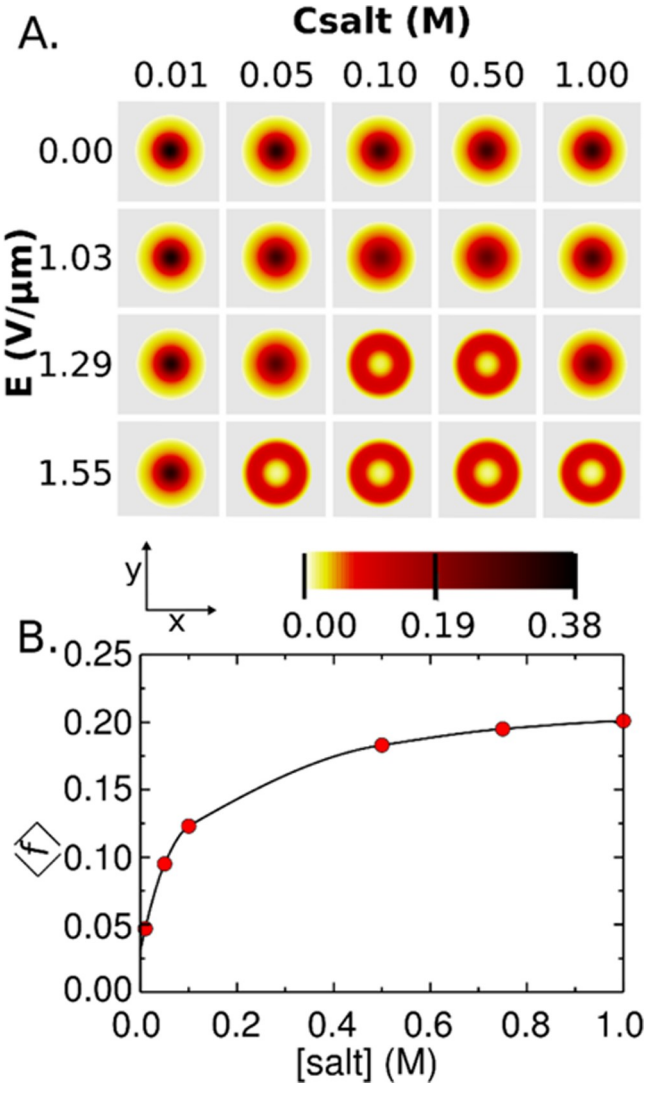

Figure 4. (A) Effect of the electric potential and salt concentration on the polymer conformation. (B) Effect of salt concentration on the average dissociation fraction of the polymer chains. Conditions: R = 5 nm, N = 28, pH = 8.5, pK_a = 8, surface coverage = 0.05 chains/nm^2

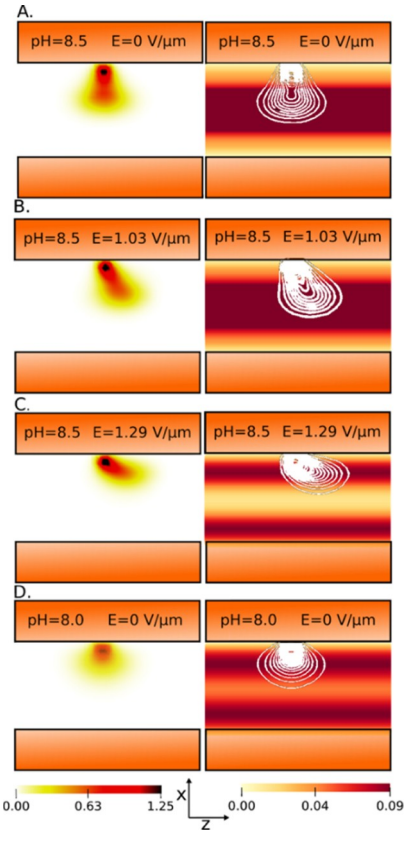

Figure 5. Color maps of the single-chain average segment densities (left panels) and total volume fraction of polyelectrolyte segments (right panels, the single-chain segment densities are overlaid as contour plots) in the (xz) plane at different applied potentials and pH: (A) pH = 8.5 and E = 0 V/μm. (B) pH = 8.5 and E = 1.03 V/μm. (C) pH = 8.5 and E = 1.29 V/μm (D) pH = 8.0 and E = 0 V/μm. Conditions: R = 5 nm, N = 28, pK_a = 8, surface coverage = 0.05 chains/nm^2, salt concentration = 0.1 M.

due to the access resistance will compete with the Ohmic drop inside the pore. In those systems, the electric field inside the pore will be smaller than ΔV/L. For polyelectrolyte-modified nanochannels similar to that discussed here, we have previously shown that the access resistances can be neglected up to L = 100 nm to 1 μm (the exact value depending on the charge of the polyelectrolyte brush[21]), which should result in threshold potentials in the range of ΔV ≃ 0.109−1.09 V. These values are well within the range of those typically used in conductance measurements. In summary, this analysis indicates that the proposed voltage-gated collapsed-to-the-center to collapsed-to-the-wall transition is feasible in current nanochannel devices.

In order to show that the change of structures observed in Figure 4 is in fact triggered by the proposed conformational rearrangements, we analyzed the average segment distribution of a single chain within the channel. Figure 5 shows color maps for the segment density of a single chain (left panels) and the volume fraction of the whole brush (right panels, the single-chain density profiles are shown as a white contour plot in this figure) in the (x, z) plane (this plane contains the channel axis, see the coordinate system in Figure 1). For a zero applied potential (Figure 5A), the polyelectrolyte chain is symmetrically distributed with respect to the normal of the surface and its density profile is elongated near the axis, as expected for a chain-forming part of the central plug. As the potential increases, the chain interacts with the electric field and deforms in the axial direction. For E = 1.03 V/μm (see Figure 5B), the chains are tilted in the direction of the field but still collapsed near the channel axis. Above the threshold potential (E = 1.29 V/μm, Figure 5C), the electrostatic coupling triggers a steep conformational rearrangement. This transition places the chains almost parallel to the wall and the layer switches to the collapsed-to-the-wall conformation. It is interesting to compare Figure 5C (E = 1.29 V/μm, pH 8.5) with Figure 5D (E = 0 V/μm, pH 8.0). In both cases, the polyelectrolyte is collapsed to the walls, but in Figure 5C, this structure is due to the external electrical field, while in Figure 5D, this structure arises from the increase in the charge of the polybase because of the decrease in pH (see Figure 3). In the latter case, the chain does not extend in the axial direction, but it is still collapsed on the wall.

Figure 4A shows that the applied potential required to switch the conformation nonmonotonically depends on the salt concentration, C_{salt}, and it has a minimum for intermediate salt concentrations (C_{salt} = 0.1 − 0.5 M). This effect is ascribed

https://dx.doi.org/10.1021/acs.macromol.0c00082
Macromolecules 2020, 53, 2616−2626

to the well-known double role that increasing electrostatic screening plays in weak polyelectrolyte systems.[43,48,55] Starting from a high-salt concentration, decreasing C_{salt} has the main effect of reducing the electrostatic screening between charged polyelectrolyte segments. Stronger segment−segment repulsions favor the collapsed-to-the-wall state over the collapsed-to-the-center one (increasing C_{salt} produces in this regime the same effect as decreasing pH; see Figure 3). A further decrease of salt concentration, on the other hand, produces the opposite effect: it stabilizes again the collapsed-to-the-center structure. This effect can be traced back to the decrease in the fraction of charged polymer segments because of the charge regulation effect. Briefly, a decrease in the salt concentration increases the electrostatic repulsions between positively charged segments. This process results in an increase in the free energy required to protonate a segment of the polybase; therefore, the acid−base equilibrium of the basic segments shifts toward the neutral state. This argument is supported by the plot of the average fraction of charged segments in the brush, $\langle f \rangle$, versus C_{salt} in Figure 4B, which shows that $\langle f \rangle$ rapidly increases with increasing C_{salt} for small salt concentrations and then plateaus for large salt concentrations. The decrease in the fraction of charged segments with decreasing C_{salt} in the low-salt-concentration regime favors the formation of the collapsed-to-the-center structure because it is the most compact structure (it has a maximum volume fraction higher than that of the collapsed-to-the-wall structure).

In previous studies of polymer brushes in poor solvent conditions, we have observed the possibility of having bistable systems in equilibrium, where the molecular theory predicted the existence of more than one local free-energy minima with very different morphologies.[55,56] In order to test whether bistability is present in the current system, we solved the molecular theory for increasing values of the applied potential until we obtained the conformational transition, and then we decreased the electric field back to the equilibrium condition (E = 0). The results of this calculation (Figure 6) show that for some values of E, two different structures can be obtained, which indicate that this system is bistable. It should be noted that our theory models a steady state; therefore, processes depicted in Figure 6 are not really a time-dependent potential scan, but rather they result from the choice of the initial guesses used to solve the molecular theory. When solving the molecular theory, we use a previous solution as an initial guess for the next calculation; therefore, solving the theory for increasing or decreasing values of E can produce different results if the system is bistable. All calculations presented so far in Figures 4 and 5 correspond to calculations where E was increased from the equilibrium system (E = 0) to the desired final value.

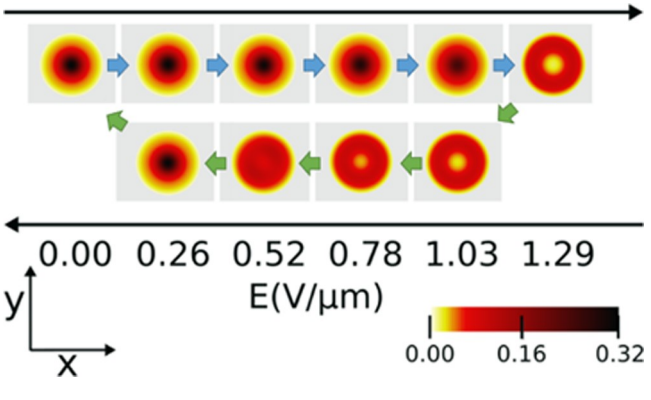

Figure 6. Color maps in the (x, y) plane of the volume fraction of the polyelectrolyte for a calculation increasing the applied electrical from E = 0.0 V/μm to E = 1.29 V/μm (forward scan, upper row) and a calculation decreasing the electric field from E = 1.29 V/μm to E = 0 V/μm (reverse scan, lower row). The plot shows the existence of bistability in the system. Same conditions as in Figure 5.

The different morphologies observed for the forward and backward scans in Figure 6 strongly suggest the possibility of hysteresis in an experimental realization of the system. The current−potential curves of many nanochannel systems exhibit hysteresis, indicating kinetic bistability.[33,34,54,57,58] In some of these systems, the bistability has been directly associated with polymer relaxation.[33,34,57]

Effect of the Polyelectrolyte Structure on Transport. In this section, we address the question of how the sharp structural transition predicted by the theory affects the transport through the channel. The total flow of a charged species i through the pore is given by (see eq S48 in the Supporting Information)

$$\Phi_{z,i} = E \int M_i(\langle \phi_P(x,y) \rangle)\, \rho_i(x,y)\, dx\, dy \tag{3}$$

where the integral runs over the cross section of the channel, the subindex "z" indicates that the flow occurs in the z direction, $\rho_i(x, y)$ is the number density of species i at position (x, y) (in the long-channel approximation, the concentrations are independent on the axial position, see the Supporting Information and Theoretical Methods section) and $M_i(\langle \phi_P(x, y) \rangle)$ is the ionic mobility of the species i, which is related to its diffusion coefficient D_i, as

$$M_i(\langle \phi_P(x,y) \rangle) = D_i(\langle \phi_P(x,y) \rangle)\, \beta q_i \tag{4}$$

where q_i is the charge of species i and $\beta = 1/k_B T$ (k_B is Boltzmann's constant and T is the temperature). Note that both D_i and M_i are allowed to depend on the local volume fraction of the polymer, $\langle \phi_P(x,y) \rangle$. Equation 3 shows that the transport rate depends in our theory on both the concentration of the transported species within the channel, ρ_i, and their mobility, M_i.

We will first discuss the effect of the collapse transition on the density of probe particles within the channel. In our theory, the concentration of a molecular species at position r within the channel is given by (see eq S45 in the Supporting Information)

$$\rho_i(x,y) = \rho_i^{bulk} \exp(-\beta v_i(\pi(x,y) - \pi^{bulk}) - q_i \beta \psi^0(x,y)) \tag{5}$$

where π(x, y) is the osmotic pressure at position (x, y), v_i is the volume of species i, and $\psi^0(x,y)$ is the electrostatic potential at a position (x, y) at the left entrance of the channel (axial position z = 0). Equation 2 is valid for very small particles, for which π(x,y) and $\psi^0(x, y)$ can be considered constant in the whole volume of the particle. For larger particles, eq 5 can be generalized to[42,59]

$$\rho_i(x,y) = \rho_i^{bulk} \exp\left(-\beta \int [v_i(x,y,\mathbf{r}')(\pi(x',y') - \pi^{bulk}) - q_i(x,y,\mathbf{r}')\beta\psi^0(x',y')]\, d\mathbf{r}'\right) \tag{6}$$

https://dx.doi.org/10.1021/acs.macromol.0c00082
Macromolecules 2020, 53, 2616−2626

where r′ = (x′, y′, z′) and $u(x, y, r')dr'$ and $q(x, y, r')dr'$ are the volume and charge, respectively, that a probe particle with its center at position (x, y) has in the volume element between r′ and r′ + dr′. Assuming that the density of the probe is small, then the fields $\psi^0(x, y)$ and $\pi(x, y)$ in the presence of the probe are approximated to be the same as those determined by solving the molecular theory in the absence of a probe.

In all our calculations, we allow the structure of the polyelectrolyte brush to depend on x and y; however, for simplicity, we choose to use solutions with angular symmetry to explore the voltage-triggered structural transition. Therefore, the solutions discussed in the previous section depended only on r, the radial coordinate. Figure 7A shows the densities of

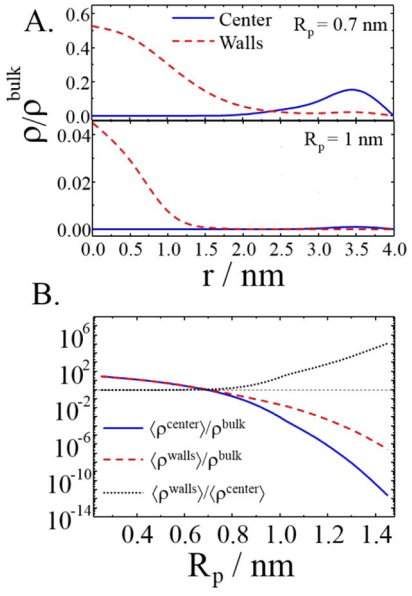

Figure 7. (A) Density of probe particles with radius R_p = 0.7 nm (upper panel) or 1.0 nm (lower panel) along the radial coordinate of the channel for two different states of the polyelectrolyte brush: the collapsed-to-the-center polymer layer (solid blue lines, corresponds to E = 1.03 V/μm) and the collapsed-to-the-wall state (dashed red lines, corresponds to E = 1.29 V/μm). (B) Relative concentration of the nanoparticle inside the nanochannel with respect to the bulk for the collapsed-to-the-center channel (solid blue line) and the collapsed-to-the-wall channel (dashed red line) and ratio of the concentrations inside channels in the two different states (short-dashed black line) as a function of the radius of the probe particle.

probe particles as a function of r within nanochannels in the collapsed-to-the-center (solid blue lines, corresponds to the system with E = 1.03 V/μm and C_{salt} = 0.1 M in Figure 4) and collapsed-to-the-wall (dashed red lines, corresponds to E = 1.29 V/μm and C_{salt} = 0.1 M) states. Results are shown for particles of two different radii (R_p = 0.7 nm and R_p = 1.0 nm) with a single negative charge located at the center. In all cases, the density of the probe is normalized by the bulk density, ρ^{bulk}. For both particle sizes, Figure 7A shows that the smallest density is obtained at the axis of the channel (r = 0) for the collapsed-to-the-center conformation and near the channel walls for the collapsed-to-the-wall case. This result indicates that steric repulsions (i.e., the first term within the integral in eq 6) dominate over electrostatic attractions (second term in the integral in eq 6). As expected from this conclusion, increasing the size of the nanoparticle decreases its local density (see density scales in the two plots of Figure 7A).

In order to evaluate the effectivity of the proposed nanomechanical gate to control the transport of particles of different sizes, we calculate the average concentration of particles within the channel,[39] which we denote $\langle\rho^k\rangle$

$$\langle\rho^k\rangle = \frac{1}{A}\int \rho(x, y)\,dx\,dy \tag{7}$$

where k = center or walls when the polyelectrolyte layer is in the collapsed-to-the-center or in collapsed-to-the-wall state, respectively (we also dropped the subscript p for clarity). The integral in eq 7 runs over the area of the channel, which is equal to A. We will study the concentration of the probe within the channel with respect to that in the bulk, that is, the partition ratio, $\langle\rho^k\rangle/\rho^{bulk}$, for k = center or walls. The partition indicates whether the probe particle is enriched, $\langle\rho^k\rangle/\rho^{bulk} > 1$, or depleted, $\langle\rho^k\rangle/\rho^{bulk} < 1$, within the channel. Small values of $\langle\rho^k\rangle/\rho^{bulk}$ will indicate small transport rates of the probe particle through the channel (poor permeability). We are also interested in the relative ratio of concentrations between the collapsed-to-the-wall and the collapsed-to-the-center structures, $\langle\rho^{walls}\rangle/\langle\rho^{center}\rangle$. This value indicates the relative selectivity of the probe particle for one of the two states. Values of $\langle\rho^{walls}\rangle/\langle\rho^{center}\rangle$ far from unity, therefore, indicate that the structural rearrangement of the polymer layer can efficiently gate the transport of the probe particle, that is, the channel will allow its passage in one configuration and block it in the other.

Figure 7B shows $\langle\rho^{walls}\rangle/\rho^{bulk}$, $\langle\rho^{center}\rangle/\rho^{bulk}$, and $\langle\rho^{walls}\rangle/\langle\rho^{center}\rangle$ (calculated using eqs 6 and 7) as a function of the radius of the particle, R_p. Probe particles with a radius smaller than 1 nm have a concentration inside the channel (for both collapse states) similar to or slightly higher than in the bulk, that is, $\langle\rho^k\rangle/\rho^{bulk} > 1$, because of the particle−brush electrostatic attractions. For particles with $R_p > 1$ nm, steric repulsions dominate and the probe concentration inside the channels is smaller than in the bulk, $\langle\rho^k\rangle/\rho^{bulk} < 1$.

The concentration ratio between the collapsed-to-the-wall and collapsed-to-the-center systems, $\langle\rho^{walls}\rangle/\langle\rho^{center}\rangle$, (solid blue line in Figure 7B), increases with increasing particle size because of the increase of steric repulsions between the particle and the central plug in the collapsed-to-the-center case. Note that this increase in selectivity comes along with a decrease in the permeability of the nanochannel, that is, a decrease of $\langle\rho^{walls}\rangle/\rho^{bulk}$. In other words, large values of $\langle\rho^{walls}\rangle/\langle\rho^{center}\rangle$ (high selectivity) occur for small values of $\langle\rho^{walls}\rangle/\rho^{bulk}$ and $\langle\rho^{center}\rangle/\rho^{bulk}$ (poor permeability) and vice versa. The balance between selectivity and permeability is a recurrent issue found in the design of synthetic nanochannels for ion separation.[60,61]

The estimations of the probe concentration within the channel shown in Figure 7 suggest that the voltage-gated transition will be inefficient to control the passage of particles with a radius smaller than 1 nm because their concentrations are very similar in both collapsed states. Because ions have R_p < 1 nm, large changes in conductance are not expected during the voltage-gated transition. This argument is based on the concentration of charge carriers in the channel and, therefore, does not consider possible changes in probe mobility triggered by the collapse transition, which is another factor that dictates the flux of particles through the channel (see eq 3). In the case of small ions, ion mobility within the polyelectrolyte-modified channel is a problem difficult to analyze, which is beyond the capabilities of our theory. Luijten and co-workers studied ion mobility in flat polyelectrolyte brushes and showed that

https://dx.doi.org/10.1021/acs.macromol.0c00082
Macromolecules 2020, 53, 2616−2626

mobility strongly depends on the density of the brush.[62] Moreover, different authors have put forward simple analytical models that relate apparent diffusion coefficients within a polymeric gel to the polymer density in the gel.[63] We attempted to use these simple models to provide an estimation of the possible effect of the voltage-gated transition on the total ion current through the channel (see the Supporting Information). In all cases, our results indicate that the changes in ion conductance due to the collapsed-to-the-center/collapsed-to-the-wall transition will be rather small (<5%). This result can be rationalized by considering that in the two collapse states the total amount of polymer is the same and the polymer aggregates have a similar volume fraction, although the position of the aggregate changes. Thus, the collapsed-to-the-center conformation blocks ions flowing through the central channel and the collapsed-to-the-wall one blocks ions flowing near the walls, but the total conductance is similar in both cases.

CONCLUSIONS

In the present work, we used a molecular theory to study the effect of an applied transmembrane potential on the conformation of a polyelectrolyte brush inside a nanochannel. The molecular theory used in this work allowed us to study a long cylindrical nanochannel in a steady state and explicitly include molecular details of the polymers grafted on the inner walls (such as their internal conformations, chain length, and segment volume), their electrostatic and nonelectrostatic interactions, and the presence of a coupled chemical equilibrium.

For polymers interacting via short-range and Coulombic segment−segment interactions, our theory predicts a transition from the collapsed-to-the-center state to the collapsed-to-the-wall structure upon increasing the applied transmembrane potential. In order to find the optimal conditions for this voltage-triggered transition, we first explored how the polymer length and the nanochannel radius direct the hydrophobicity-driven collapse to one of these two states. We then explored the effect of pH to find a condition where a small pH change triggers the conformational transition.

We explored the effect of the brush conformation on the partition of particles of different sizes between the channel and the bulk solution in order to analyze if the voltage-triggered collapse transition can gate the transport of these particles. We found that small particles (R_p < 1 nm, e.g., salt ions) can easily permeate into the nanochannels (i.e., their concentration in the channel is larger than or equal to the bulk concentration), but there is poor selectivity between the collapsed-to-the-wall and the collapsed-to-the-center states. On the other hand, large probe particles (R_p > 1 nm) exhibit good selectivity for the collapsed-to-the-wall state, but their concentration within the channel is predicted to be significantly smaller than the bulk one, and therefore, their permeation rate will be slow. The competition between selectivity and permeability is a recurrent theme in synthetic nanochannels and a challenge that should be overcome in order to reach the performance of biological systems.[64−66] In the present case, a reasonable selectivity/permeability balance can be achieved for particles with radii in the ~1 nm range.

The field of nanofluidics is quickly evolving thanks to the combination of new fabrication and surface modification tools, the development of groundbreaking applications, and a solid theoretical foundation based on our understanding of ion and solvent transport. Extending these theoretical efforts to systems including soft and biomaterials is challenging because of their molecular complexity, but it is also a highly attractive and potentially rewarding research direction which will enable the design of novel smart nanofluidic devices.

ASSOCIATED CONTENT

Supporting Information

The Supporting Information is available free of charge at https://pubs.acs.org/doi/10.1021/acs.macromol.0c00082.

Detailed description of the theoretical methods and molecular model (PDF)

AUTHOR INFORMATION

Corresponding Authors

Igal Szleifer − Department of Biomedical Engineering, Department of Chemistry and Chemistry of Life Processes Institute, Northwestern University, Evanston, Illinois 60208, United States; orcid.org/0000-0002-8708-0335; Email: igalsz@northwestern.edu

Mario Tagliazucchi − INQUIMAE-CONICET and DQIAQF, University of Buenos Aires, School of Sciences, Buenos Aires C1428EHA, Argentina; orcid.org/0000-0003-4755-955X; Email: mario@qi.fcen.uba.ar

Author

Yamila A. Perez Sirkin − INQUIMAE-CONICET and DQIAQF, University of Buenos Aires, School of Sciences, Buenos Aires C1428EHA, Argentina

Complete contact information is available at: https://pubs.acs.org/10.1021/acs.macromol.0c00082

Author Contributions

The manuscript was written through contributions of all authors.

Notes

The authors declare no competing financial interest.

ACKNOWLEDGMENTS

M.T. is a fellow of CONICET. Y.P.S. acknowledges a CONICET postdoctoral scholarship. M.T. acknowledges financial support from Agencia Nacional de Promoción Científica y Tecnológica (ANPCyT) PICT-0099-2015 and PICT 0154-2016 and University of Buenos Aires (UBACYT 20020170200215BA). I.S. acknowledges support from NSF, Div. of Chem. Bioeng. Env. and Transp. Sys. 1833214.

REFERENCES

(1) Doyle, D. A.; Cabral, J. M.; Pfuetzner, R. A.; Kuo, A.; Gulbis, J. M.; Cohen, S. L.; Chait, B. T.; MacKinnon, R. The Structure of the Potassium Channel: Molecular Basis of K+ Conduction and Selectivity. Science 1998, 280, 69−77.

(2) Lim, C.; Dudev, T. Potassium Versus Sodium Selectivity in Monovalent Ion Channel Selectivity Filters. In The Alkali Metal Ions: Their Role for Life; Sigel, A., Sigel, H., Sigel, R. K.O., Eds.; Metal Ions in Life Sciences; Springer International Publishing: Cham, 2016; pp 325−347.

(3) Schreiber, M.; Wei, A.; Yuan, A.; Gaut, J.; Saito, M.; Salkoff, L. Slo3, a Novel pH-Sensitive K+ Channel from Mammalian Spermatocytes. J. Biol. Chem. 1998, 273, 3509−3516.

(4) Kass, I.; Arkin, I. T. How pH Opens a H+ Channel: The Gating Mechanism of Influenza A M2. Structure 2005, 13, 1789−1798.

https://dx.doi.org/10.1021/acs.macromol.0c00082
Macromolecules 2020, 53, 2616−2626

(5) Jensen, M. L.; Schousboe, A.; Ahring, P. K. Charge Selectivity of the Cys-Loop Family of Ligand-Gated Ion Channels. J. Neurochem. 2005, 92, 217−225.
(6) Keramidas, A.; Moorhouse, A. J.; Schofield, P. R.; Barry, P. H. Ligand-Gated Ion Channels: Mechanisms Underlying Ion Selectivity. Prog. Biophys. Mol. Biol. 2004, 86, 161−204.
(7) Chung, S.-H.; Anderson, O. S.; Krishnamurthy, V. V. Biological Membrane Ion Channels: Dynamics, Structure, and Applications; Springer Science & Business Media, 2007.
(8) Murata, K.; Mitsuoka, K.; Hirai, T.; Walz, T.; Agre, P.; Heymann, J. B.; Engel, A.; Fujiyoshi, Y. Structural Determinants of Water Permeation through Aquaporin-1. Nature 2000, 407, 599−605.
(9) Hille, B. Ionic Channels in Excitable Membranes. Current Problems and Biophysical Approaches. Biophys. J. 1978, 22, 283−294.
(10) Huang, J.; Zhang, X.; McNaughton, P. A. Modulation of Temperature-Sensitive TRP Channels. Semin. Cell Dev. Biol. 2006, 17, 638−645.
(11) Xiao, K.; Wen, L.; Jiang, L. Biomimetic Solid-state Nanochannels: From Fundamental Research to Practical Applications. Small 2016, 12, 2810−2831.
(12) Ding, D.; Gao, P.; Ma, Q.; Wang, D.; Xia, F. Biomolecule-Functionalized Solid-State Ion Nanochannels/Nanopores: Features and Techniques. Small 2019, 15, 1804878.
(13) Zhang, H.; Tian, Y.; Jiang, L. Fundamental Studies and Practical Applications of Bio-Inspired Smart Solid-State Nanopores and Nanochannels. Nano Today 2016, 11, 61−81.
(14) Pérez-Mitta, G.; Toimil-Molares, M. E.; Trautmann, C.; Marmisollé, W. A.; Azzaroni, O. Molecularly Designed Solid-State Nanopores: Fundamental Concepts and Applications. Adv. Mater. 2019, 0, 1901483.
(15) Tagliazucchi, M.; Szleifer, I. Chemically Modified Nanopores and Nanochannels; William Andrew, 2016.
(16) Siwy, Z. S. Ion-Current Rectification in Nanopores and Nanotubes with Broken Symmetry. Adv. Funct. Mater. 2006, 16, 735−746.
(17) Daiguji, H. Ion Transport in Nanofluidic Channels. Chem. Soc. Rev. 2010, 39, 901−911.
(18) Ali, M.; Nasir, S.; Ensinger, W. Bioconjugation-Induced Ionic Current Rectification in Aptamer-Modified Single Cylindrical Nanopores. Chem. Commun. 2015, 51, 3454−3457.
(19) Ramírez, P.; Gómez, V.; Cervera, J.; Schiedt, B.; Mafé, S. Ion Transport and Selectivity in Nanopores with Spatially Inhomogeneous Fixed Charge Distribution. J. Chem. Phys. 2007, 126, 194703.
(20) Siwy, Z.; Kosińska, I. D.; Fuliński, A.; Martin, C. R. Asymmetric Diffusion through Synthetic Nanopores. Phys. Rev. Lett. 2005, 94, 048102.
(21) Yameen, B.; Ali, M.; Ramírez, R.; Ensinger, W.; Knoll, W.; Azzaroni, O. Single Conical Nanopores Displaying PH-Tunable Rectifying Characteristics. Manipulating Ionic Transport with Zwitterionic Polymer Brushes. J. Am. Chem. Soc. 2009, 131, 2070−2071.
(22) Ali, M.; Yameen, B.; Neumann, R.; Ensinger, W.; Knoll, W.; Azzaroni, O. Biosensing and Supramolecular Bioconjugation in Single Conical Polymer Nanochannels. Facile Incorporation of Biorecognition Elements into Nanoconfined Geometries. J. Am. Chem. Soc. 2008, 130, 16351−16357.
(23) Siwy, Z.; Trofin, L.; Kohli, P.; Baker, L. A.; Trautmann, C.; Martin, C. R. Protein Biosensors Based on Biofunctionalized Conical Gold Nanotubes. J. Am. Chem. Soc. 2005, 127, 5000−5001.
(24) Cervera, J.; Schiedt, B.; Ramirez, P. A Poisson/Nernst-Planck Model for Ionic Transport through Synthetic Conical Nanopores. Europhys. Lett. 2005, 71, 35.
(25) Cao, L.; Guo, W.; Wang, Y.; Jiang, L. Concentration-Gradient-Dependent Ion Current Rectification in Charged Conical Nanopores. Langmuir 2012, 28, 2194−2199.
(26) Schoch, R. B.; Han, J.; Renaud, P. Transport Phenomena in Nanofluidics. Rev. Mod. Phys. 2008, 80, 839.
(27) Yameen, B.; Ali, M.; Neumann, R.; Gómez, W.; Knoll, W.; Azzaroni, O. Synthetic Proton-Gated Ion Channels via Single Solid-State Nanochannels Modified with Responsive Polymer Brushes. Nano Lett. 2009, 9, 2788−2793.
(28) Guo, W.; Xia, H.; Xia, F.; Hou, X.; Cao, L.; Wang, L.; Xue, J.; Zhang, G.; Song, Y.; Zhu, D.; et al. Current Rectification in Temperature-Responsive Single Nanopores. ChemPhysChem 2010, 11, 859−864.
(29) Nasir, S.; Ali, M.; Ensinger, W. Thermally Controlled Permeation of Ionic Molecules through Synthetic Nanopores Functionalized with Amine-Terminated Polymer Brushes. Nanotechnology 2012, 23, 225502.
(30) Nasir, S.; Ali, M.; Ramirez, P.; Gómez, V.; Oschmann, B.; Muench, F.; Tahir, M. N.; Zentel, R.; Mafe, S.; Ensinger, W. Fabrication of Single Cylindrical Au-Coated Nanopores with Non-Homogeneous Fixed Charge Distribution Exhibiting High Current Rectifications. ACS Appl. Mater. Interfaces 2016, 8, 12486−12494.
(31) Tagliazucchi, M.; Rabin, Y.; Szleifer, I. Ion Transport and Molecular Organization Are Coupled in Polyelectrolyte-Modified Nanopores. J. Am. Chem. Soc. 2011, 133, 17753−17763.
(32) Harrell, C. C.; Kohli, P.; Siwy, Z.; Martin, C. R. DNA−Nanotube Artificial Ion Channels. J. Am. Chem. Soc. 2004, 126, 15646−15647.
(33) Nguyen, G.; de la Cruz, M. O.; Siwy, Z. S. DNA Strands Attached inside Single Conical Nanopores: Ionic Pore Characteristics and Insight into DNA Biophysics. J. Membr. Biol. 2011, 239, 105−113.
(34) Buchsbaum, S. F.; Nguyen, G.; Kroger, S.; Siwy, Z. S. DNA-Modified Polymer Pores Allow PH-and Voltage-Gated Control of Channel Flux. J. Am. Chem. Soc. 2014, 136, 9902−9905.
(35) Sigworth, F. J. Life's transistors. Nature 2003, 423, 21.
(36) Tagliazucchi, M.; Olvera de la Cruz, M.; Szleifer, I. Self-Organization of Grafted Polyelectrolyte Layers via the Coupling of Chemical Equilibrium and Physical Interactions. Proc. Natl. Acad. Sci. U.S.A. 2010, 107, 5300−5305.
(37) Peleg, O.; Tagliazucchi, M.; Kroger, M.; Rabin, Y.; Szleifer, I. Morphology Control of Hairy Nanopores. ACS Nano 2011, 5, 4737−4747.
(38) Osmanović, D.; Kerr-Winter, M.; Eccleston, R.; Hoogenboom, B.; Ford, I. Effects of Rotational Symmetry Breaking in Polymer-Coated Nanopores. J. Chem. Phys. 2015, 142, 034901.
(39) Speyer, K.; Pastorino, C. Pressure Responsive Gating in Nanochannels Coated by Semiflexible Polymer Brushes. Soft Matter 2019, 15, 937−946.
(40) Schepelina, O.; Zharov, I. PNIPAAM-Modified Nanoporous Colloidal Films with Positive and Negative Temperature Gating. Langmuir 2007, 23, 12704−12709.
(41) Tagliazucchi, M.; Azzaroni, O.; Szleifer, I. Responsive Polymers End-Tethered in Solid-State Nanochannels: When Nanoconfinement Really Matters. J. Am. Chem. Soc. 2010, 132, 12404−12411.
(42) Tagliazucchi, M.; Rabin, Y.; Szleifer, I. Transport Rectification in Nanopores with Outer Membranes Modified with Surface Charges and Polyelectrolytes. ACS Nano 2013, 7, 9085−9097.
(43) Gong, P.; Genzer, J.; Szleifer, I. Phase Behavior and Charge Regulation of Weak Polyelectrolyte Grafted Layers. Phys. Rev. Lett. 2007, 98, 018302.
(44) Tagliazucchi, M.; Calvo, E. J.; Kroger, I. Molecular Theory of Chemically Modified Electrodes by Redox Polyelectrolytes under Equilibrium Conditions: Comparison with Experiments. J. Phys. Chem. C 2008, 112, 458−471.
(45) Prigogine, I. Introduction to Thermodynamics of Irreversible Processes; Interscience Publishers, 1961; Vol. 31.
(46) Lebon, G.; Jou, D.; Casas-Vázquez, J. Understanding Non-Equilibrium Thermodynamics; Springer, 2008; Vol. 295.
(47) Peleg, O.; Tagliazucchi, M.; Kroger, M.; Rabin, Y.; Szleifer, I. Morphology Control of Hairy Nanopores. ACS Nano 2011, 5, 4737−4747.
(48) Zaldivar, G.; Vemulapalli, S.; Udumula, V.; Conda-Sheridan, M.; Tagliazucchi, M. Self-Assembled Nanostructures of Peptide Amphiphiles: Charge Regulation by Size Regulation. J. Phys. Chem. C 2019, 123, 17606−17615.

https://dx.doi.org/10.1021/acs.macromol.0c00082
Macromolecules 2020, 53, 2616−2626

(49) Gilles, F. M.; Tagliazucchi, M.; Azzaroni, O.; Szleifer, I. Ionic Conductance of Polyelectrolyte-Modified Nanochannels: Nanoconfinement Effects on the Coupled Protonation Equilibria of Polyprotic Brushes. J. Phys. Chem. C 2016, 120, 4789.
(50) Vlassiouk, I.; Smirnov, S.; Siwy, Z. Ionic Selectivity of Single Nanochannels. Nano Lett. 2008, 8, 1978−1985.
(51) Viasnoff, V.; Bockelmann, U.; Meller, A.; Isambert, H.; Laufer, L.; Tsori, Y. Localized Joule-Heating Produced by Ion Current Focusing through Micron-Size Holes. Appl. Phys. Lett. 2010, 96, 163701.
(52) Wu, Y.; Cheng, G.; Katsov, K.; Sides, S. W.; Wang, J.; Tang, J.; Fredrickson, G. H.; Moskovits, M.; Stucky, G. D. Composite Mesostructures by Nano-Confinement. Nat. Mater. 2004, 3, 816−822.
(53) Zhang, J.; Liu, N.; Wei, B.; Ou, X.; Xu, X.; Lou, X.; Xia, F. The Opposite Gating Behaviors of Solid-State Nanochannels Modified with Long and Short Polymer Chains. Chem. Commun. 2015, 51, 10146−10149.
(54) Sheng, Q.; Xie, Y.; Li, J.; Wang, X.; Xue, J. Transporting an Ionic-Liquid/Water Mixture in a Conical Nanochannel: A Nanofluidic Memristor. Chem. Commun. 2017, 53, 6125−6127.
(55) Tagliazucchi, M.; Li, X.; Olvera de la Cruz, M.; Szleifer, I. Self-Organized Polyelectrolyte End-Grafted Layers Under Nanoconfinement. ACS Nano 2014, 8, 9998−10008.
(56) Gleria, I.; Mocskos, E.; Tagliazucchi, M. Minimum Free-Energy Paths for the Self-Organization of Polymer Brushes. Soft Matter 2017, 13, 2362−2370.
(57) Li, Y.; Du, G.; Mao, G.; Guo, J.; Zhao, J.; Wu, R.; Liu, W. Electrical Field Regulation of Ion Transport in Polyethylene Terephthalate Nanochannels. ACS Appl. Mater. Interfaces 2019, 11, 38055−38060.
(58) Powell, M. R.; Sullivan, M.; Vlassiouk, I.; Constantin, D.; Sudre, O.; Martens, C. C.; Eisenberg, R. S.; Siwy, Z. S. Nanoprecipitation-Assisted Ion Current Oscillations. Nat. Nanotechnol. 2008, 3, 51.
(59) Tagliazucchi, M.; Szleifer, I. How Does Confinement Change Ligand−Receptor Binding Equilibrium? Protein Binding in Nanopores and Nanochannels. J. Am. Chem. Soc. 2015, 137, 12539−12551.
(60) Gin, D. L.; Noble, R. D. Designing the Next Generation of Chemical Separation Membranes. Science 2011, 332, 674−676.
(61) Wang, M.; Shen, W.; Ding, S.; Wang, X.; Wang, Z.; Wang, Y.; Liu, F. A Coupled Effect of Dehydration and Electrostatic Interactions on Selective Ion Transport through Charged Nanochannels. Nanoscale 2018, 10, 18821−18828.
(62) Yuan, J.; Antila, H. S.; Luijten, E. Dielectric Effects on Ion Transport in Polyelectrolyte Brushes. ACS Macro Lett. 2019, 8, 183−187.
(63) Amsden, B. Solute Diffusion within Hydrogels. Mechanisms and Models. Macromolecules 1998, 31, 8382−8395.
(64) Guo, Y.; Ying, Y.; Mao, Y.; Peng, X.; Chen, B. Polystyrene Sulfonate Threaded through a Metal−Organic Framework Membrane for Fast and Selective Lithium-ion Separation. Angew. Chem., Int. Ed. 2016, 55, 15120−15124.
(65) Wang, P.; Wang, M.; Liu, F.; Ding, S.; Wang, X.; Du, G.; Liu, J.; Apel, P.; Kluth, P.; Trautmann, C. Ultrafast Ion Sieving Using Nanoporous Polymeric Membranes. Nat. Commun. 2018, 9, 569.
(66) Wen, Q.; Yan, D.; Liu, F.; Wang, M.; Ling, Y.; Wang, P.; Kluth, P.; Schauries, D.; Trautmann, C.; Apel, P. Highly Selective Ionic Transport through Subnanometer Pores in Polymer Films. Adv. Funct. Mater. 2016, 26, 5796−5803.

https://dx.doi.org/10.1021/acs.macromol.0c00082
Macromolecules 2020, 53, 2616−2626